Simple Hurricane Model: Asymmetry and Dynamics

David Mendes (david.mendes@ufrn.br)

Federal University of Rio Grande do Norte Exact and Earth Sciences Centre: Universidade Federal do Rio Grande do Norte Centro de Ciencias Exatas e da Terra https://orcid.org/0000-0003-1418-5109

José Francisco de Oliveira Júnior

Federal University of Alagoas: Universidade Federal de Alagoas

Monica Cristina Damião Mendes

State University of Rio Grande do Norte: Universidade do Estado do Rio Grande do Norte

Washington Luiz Félix Correia Filho

Federal University of Rio Grande: Universidade Federal do Rio Grande

Research Article

Keywords: Tropical Cyclone, Hurricane Model, Atmospheric Dynamics

Posted Date: December 1st, 2021

DOI: https://doi.org/10.21203/rs.3.rs-1051026/v1

SIMPLE HURRICANE MODEL: ASYMMETRY AND DYNAMICS

David Mendes[1,2], José Francisco de Oliveira Júnior[3], Monica Cristina Damião Mendes[4], Washington Luiz Félix Correia Filho[5,6]

[1]Climate Sciences Post-Graduate Program, Department of Climate and Atmospheric Sciences, Federal University of Rio Grande do Norte, [2]Aerospace Engineering Post-Graduate Program, Federal University of Rio Grande do Norte, [3]Laboratory of Applied Meteorology and Environment (LAMMA), Institute of Atmospheric Sciences (ICAT), Federal University of Alagoas (UFAL), [4]Federal University of Rio Grande do Norte [5]Institute of Mathematics, Statistics, and Physics, Federal University of Rio Grande

Corresponding author
David Mendes
david.mendes@ufrn.br
Climate Sciences Post-Graduate Program, Department of Climate and Atmospheric Sciences, Federal University of Rio Grande do Norte, Lagoa Nova Campus, P.O. 1524, Natal 59078-970, Brazil

ABSTRACT

In recent decades, the development of several products and hurricane-related models has attempted to predict the dynamic conditions of these systems and regions beyond they can impact. Thus, this article presents a parametric model to describe wind asymmetry in these systems. For this, the analysis of this model was applied in Hurricane Ike, which occurred in September 2008. In this model, the tangential wind field above the boundary layer was considered in balance with the thermal wind. It was possible to identify that as Hurricane Ike evolves, tangential velocity also evolves. Thus, there was a change in static, baroclinic, and inertial stability. An exponential radial reduction was included for maximum speed, and, therefore, the maximum winds always to the right of the hurricane displacement were identified. In addition, pumping near the surface had an influx into this system induced caused by drag between the air and the surface.

Keywords: Tropical Cyclone, Hurricane Model, Atmospheric Dynamics

1. INTRODUCTION

In the last four decades, numerical models of Numerical Weather Prediction (NWP) and climate have evolved significantly, mainly in the design of new parameterizations and development of numerical codes, as well as computational advances with the advent of High-Performance Computing (*HPC*) - (Bauer et al., 2015; Váňa et al., 2017). The NWP and climate models are described by differential equations representing variability in time and space (Kalnay, 2003; Warner, 2010). These models can identify and track hurricanes and, therefore, evaluate the disasters caused in the economic and environmental sphere (Osuri et al., 2013; Luitel et al., 2018).

In recent years, several studies have pointed out that the damage caused by tropical cyclones (such as storms, ocean waves, and floods) depends heavily on the extent of maximum winds, in addition to the interference of climate change (Powell and Reinhold, 2007; Zhao and Held, 2010; Knutson et al., 2019; Knutson et al., 2020).

Tropical cyclones are usually associated with hurricanes with high-energy, highly destructible weather systems that cause massive material damage in coastal areas that exceed one billion dollars a year, as well as loss of human life (Knutson et al., 2019; Martinez, 2020).

Thus, the numerical representation of maximum winds is fundamental for a more realistic definition of both systems preceding this event and the intensity of tropical cyclones. In the 1980s, Holland (1980) proposed a parametric radial profile of hurricane winds, being the basis for a broad study regarding the intensity of tropical cyclones. Chavas and Lin (2016) developed a simple physical model for the radial structure of the azimuthal wind at low levels within a hurricane, identifying that wind variability was directly linked to its external parameters, for example, the maximum wind speed and maximum wind

radius. Previously, Smith (1980) and Tang and Emanuel (2012) identified that the most turbulent aspect of a hurricane might be associated with changes as opposed to the radius of maximum winds (Vigh et al., 2012).

A parametric representation of the pressure and wind fields in tropical cyclones, hurricanes, and typhoons facilitated the robust representation of these atmospheric systems (Schloemer, 1954; Bryan and Rotunno, 2009; Vickery, 2015). In addition, the behavior and relationships between the various parameters, for example, pressure decay, maximum speed, and maximum wind speed radius, contribute to a better understanding of tropical cyclones (Willoughby and Rahn, 2004). Vickery et al. 2009 mentioned that parametric models assist in constructing synthetic storm systems to allow the modeling of intense winds. Moreover, Olfateh et al. (2017) identified that winds from tropical cyclones, hurricanes, and typhoons could change from a perfectly asymmetric vortex movement to an asymmetric, radial, and/or azimuthal with the system's eye.

It is important to highlight that the presence of asymmetric convection due to the friction of the lower Planetary Boundary Layer (*PBL*), the southern gradients of Coriolis acceleration aid the generation or intensification of wind and pressure asymmetry in the system (Holland, 1980; Olfateh et al., 2017). However, these models lack parameters for describing asymmetric properties for tropical cyclones, such as maximum wind (Vickery and Wadhera, 2008; Olfateh et al., 2017). Therefore, a parametric model with greater precision can improve studies on tropical cyclones. For example, Xie et al. (2011) investigated the effects of wind asymmetry in four hurricanes and identified that 30% of the measured data presented wind asymmetry, contributing to an increase of up to 16% in the height of ocean waves associated with severe storms.

Several empirical formulations existing in the literature use the calculation of the maximum radius (Rmax) under asymmetric conditions (Knaff et al., 2007; Takagi et al.,

2012). Among these methods, the one proposed by Xie et al. (2006) introduced significant wind rays in four quadrants, defined as R34, R50, R64, and Rmax, in which the first three were used to estimate Rmax. On the other hand, tropical cyclones, hurricanes, and typhoons have a wind structure based on two components in the Northern Hemisphere (NH): i) the anti-clockwise rotation of the wind in the southern sector on the surface and ii) the speed of translation of the storm (Elsner et al., 1999). This method has already been used in the literature by Lin and Chavas (2012) and Chavas et al. (2015), as they mathematically merged existing theoretical solutions for the radial wind structure at the top of PBL in the hurricane's internal ascending region. The authors used the solution Emanuel and Ratunno (2011) proposed, where the convective transfer of moisture and heat was persistent. The Emanuel solution (2004) was used for external convection to which the convection was absent.

The model proposed by Hu et al. (2012) consists of a parametric wind model for a hurricane based on asymmetric vortex models (Holland, 1980). The authors included the impact of Coriolis deflection on the hurricane shape parameter. In addition, they the speed of translation of hurricanes prior to the application vortex Holland model (1980) to avoid excessive wind asymmetry.

The present study proposes parametric formulations to evaluate spatial and punctual monitoring of tropical cyclones, hurricanes, and typhoons based on the above. The study applied is based on Hurricane Ike, which occurred in the North Atlantic in September 2008.

2. TROPICAL CYCLONE IKE

Hurricane Ike originated from a tropical wave on September 1st of 2008, about 775 miles west of the Cape Verde archipelago. The depression quickly intensified into a tropical storm, which became a hurricane on September 3rd of 2008, with its peak intensity on

September 4th of 2008. Winds were estimated to reach 123 kt (*category 4*) when it was located 550 miles northeast (NE) from the Leeward Islands. However, Ike weakened and regained its Category 4 hurricane status shortly before hitting the Turks and Caicos Islands on September 7th of 2008 (NHC, 2008).

Hurricane Ike turned into the West direction (*W*), hitting Cuba's NE coast early on September 8th of 2008, with maximum winds at 117 kt, category 4. On the same day, Ike moved toward the Mexican coast, with winds of 69 kt (*category 1*), which intensified over the Gulf of Mexico, where it moved northwest (NW). Then it gradually intensified when crossing the Gulf of Mexico toward the coast of Texas, USA. Finally, Ike hit the US coast on the morning of September 13th, being category 2, with winds of up to 95 kt. After entering the continent, Hurricane Ike weakened, becoming an extratropical cyclone (NHC, 2008).

2.1 DAMAGES CAUSED BY THE HURRICANE IKE

Hurricane Ike left a trail of deaths and destruction, killing 74 people in Haiti and two in the Dominican Republic. The Turks and Caicos Islands and the Southeastern (SE) of the Bahamas suffered widespread damage, where seven deaths were recorded in Cuba. In addition, Ike devastated the Bolivar Peninsula – Texas/USA, with huge waves and intense winds responsible for flooding and property damage to homes and buildings. Twenty-one people died in the United States, mainly in Texas, Louisiana, and Arkansas. In the Florida Keys, approximately 15,000 people were evacuated as Hurricane Ike approached the coast. The damage caused by Hurricane Ike was estimated at over US$60 million in the Turks and Caicos Islands, between US$50 million and US$200 million in the Bahamas, and between US$3 billion and US$4 billion in Cuba (NHC, 2008).

3. MODEL IDEALIZATION

3.1 CONTEXTUALIZATION

Previously, several models used analytical parametric formulations that represent radial wind profiles in tropical cyclones (Holland et al., 2010). The schemes are "*parametric*" when the variation of the radial wind depends only on some parameters, such as maximum wind, maximum wind radius, and central pressure (Holland et al., 1984; Holland et al., 2010). The simplicity, computational cost, and spatial resolution favor the use of parametric winds to assess wind return periods in tropical cyclones, hurricanes, and typhoons and still manage to model the risk of these events (Vickery and Twisdale, 1995; Holland et al., 2010; Bhardwaj et al., 2020). The equations mentioned here explore the basic structure of hurricanes, in which surface pressure decreases exponentially toward the center of the hurricane and stabilizes in the hurricane's eye. However, winds increase exponentially in reverse toward the eye wall. Schloemer (1954) mentioned that the radial wind evolved the formulation of Rankine's combined vortex, in which the rotation of a solid body is assumed within the eye wall, and thus, tangential winds decrease on a radial scale to a rectangular hyperbolic approach. Therefore, this article will use the scheme proposed by Holland (1980), in which the radial wind profile presents significant variations in the winds of tropical cyclones. Holland (1980) modified the equation proposed by Scholoemer (1954) to represent a spectrum of rectangular hyperbole with pressure variation.

Although widely used, the formulation proposed by Holland (1980) is known for presenting some limitations, one of which is the non-representation of the walls of the Hurricane eye in a double way. Another limitation is the inability to accurately represent the winds of the eye wall and the external core simultaneously, on the other hand, it can identify the external wind profile with some precision but fails to capture the rapid decrease of wind outside the eye wall, which in several cases occurs the underestimation

of the maximum wind (*Vmax*). However, the greatest limitation scan of Holland's model (1980) is 2D projection, which implies symmetrical vortices. Unfortunately, winds in tropical cyclones are rarely symmetrical, especially when the system enters the Earth's surface. Xie et al. (2006) improved Holland's model (1980) by considering asymmetry. Then, Mattocks and Forbes (2008) developed an asymmetric wind model based on Xie et al. (2006), in which they employ a storm wave model. In this model, the authors replaced Rm with a directionally variable (*Rm(h)*), where h is the azimuthal angle around the storm's center, improving the wind field estimation in tropical cyclones.

4. IDEALIZED MODEL

As a premise of the entire dynamic model, it is necessary to introduce initial conditions for its proper functioning. In this case, reanalysis data ERA5 was used as an entry condition (Hersbach et al., 2020). The variables used as initial conditions were: i) Sea-Level Pressure (*SLP, kPa*), zonal (*u,* $m.s^{-1}$) and meridional (*v,* $m.s^{-1}$) winds (all levels), Air temperature (*Tair, ºC*) - (all levels), Relative Humidity (*RH, %*) - (all levers) and Sea Surface Temperature (*SST, ºC*). In spatial discretization, the values and derivatives of the variables used in the model were represented in discrete points on a regular grid, with Latitude (*Lat, º*) and Longitude (*Lon, º*). It is noteworthy that the spectral method was used once that it has advantages of calculating the differential terms of dynamic conditions, with a spacing of 0.5° latitude and longitude and an integration of 6 hours in time.

4.1 INITIAL SPIN UP

Systems associated with supercells, such as tornadoes, are formed by the horizontal wind inclination, while tropical cyclones are associated with convergence, i.e., rotation is

always towards the low center (Kalourazi et al., 2020). During convergence, the angular momentum associated with the Earth's rotational motion is concentrated at the angular momentum and, therefore, associated with the hurricane's winds. Thus, the calculation of the absolute angular momentum is given by Eq. (1):

$$AM = V_{tan} \cdot R + \frac{1}{2} f_c \cdot R^2 \quad (1)$$

Where, V_{tan} ($m.s^{-1}$) is the tangential velocity in an R (km) radius of the hurricane center (Harasti, 2003) and f_c (s^{-1}) is the Coriolis parameter. Thus, Eq. (1) shows the absolute angular momentum, meaning that this amount includes the relative angular momentum of the hurricane, followed by the angular momentum associated with the Earth's rotational motion.

This angular moment would be conserved if tropical cyclones did not experience surface friction as long as the air converged. Thus, the tangential wind velocity (V_{tan}) in a smaller radius (R_{final}) could be created even if the air in some initial radius (R_{init}) did not have rotation ($V_{tan_{init}} = 0$). Therefore, the formulation was added to the model, in Eq.(2):

$$V_{tan} = \frac{f_c}{2} \cdot \left(\frac{R_{init}^2 - R_{final}^2}{R_{final}}\right) \quad (2)$$

In tropical cyclones, it is known that frictional drag cannot be overlooked (Malkus and Riehl, 1960; Wood and White, 2011). Thus, tangential winds are smaller than those calculated in Eq. (2).

As wind acceleration in a hurricane intensifies, centrifugal force gains importance. Therefore, it is important to include in the model of the pressure gradient formulation, given by Eq. (3):

$$\frac{\Delta p}{\Delta R} \cdot \frac{1}{\rho} = f_c \cdot V_{tan} + \frac{V_{tan}^2}{R} \quad (3)$$

where, $\frac{\Delta p}{\Delta R}$ is the radial pressure gradient and ρ is the air density. The last term ($\frac{V_{tan}^2}{R}$) represents centrifugal force.

Moreover, the gradient wind applies to all radius of the center storms, associated with the hurricane, and all latitudes. Except in the proximity of the bottom, within the PBL and in the top clouds (Yoshizumi, 1968; Wang et al., 2017).

For a rough approach, it is important to overlook the strength of Coriolis in the vicinity of the center of the most intense hurricanes, where winds are fast, however, the idea that the cyclotrophic wind can approach the tangential winds of the hurricane was introduced, Eq.(4):

$$V_{ciclo} = V_{tan} \tag{4}$$

This implies:

$$V_{tan} = \left(\frac{R}{\rho} \cdot \frac{\Delta P}{\Delta R}\right)^{\frac{1}{2}} \tag{5}$$

In a hurricane, the shallow drag of the sea causes the winds to spiral toward the eye wall. The gradient wind equation in PBL describes this flow well. If there was no such drag-related influx, the storms on the eyewall would not get hot and humid air, which would result in the hurricane dissipates. An important process is related to the upward storm currents in the eye wall, which move, and the air rises rapidly. In this way, the output is related to the air that moves cyclically from the PBL and is driven to the top of the hurricane by air currents in the eye wall quickly that its inertia, preventing it from changing instantly to an anticyclonic flow, that is, the output flow is initially moving in the wrong direction and around the top of the system.

The center of a hurricane is hotter than the surrounding air, and this occurs due to the release of latent heat (*LH*) by organized convection and adiabatic heating due to subsidence in the system's eye. In this way, the air rises adiabatically moist in the storm cluster, but after losing water due to precipitation, the air descends more adiabatically dry in the system’s eye.

It is known that a hurricane has a warm core and is surrounded by cold air. This thermal gradient, called the radial temperature gradient, causes a reversal of the pressure gradient with the increase of the altitude due to the thermal wind (Hart, 2003).

Thus, to determine this pressure gradient, the pressure at sea level in the hurricane's eye was defined as P_b, and in the surroundings, as $P_{b\infty}$ tends to infinity (∞). At the top of the hurricane, it was set the central pressure with P_t, and around as already mentioned for P_b, the pressures tend to infinite $P_{t\infty}$.

Thus, the pressure gradient (ΔP) at the top is: $\Delta P_t = P_{t\infty} - P_{te}$, i.e., the difference between the pressure at the top tending to infinity, minus the pressure at the top of the eye, so the proportionality between the pressure on the surface or base (suffix b): $\Delta P_b = P_{b\infty} - P_{be}$, so:

$$\Delta P_t \approx a \cdot \Delta P_b - b \cdot \Delta T \quad (6)$$

In which, $a = 0.15$, being one-dimensional, $b = 0.7\ kPa/K$ ($7\ hPa/K$), and $\Delta T = T_e - T_\infty$ being the average temperature difference along the troposphere and thermal gradient (ΔT) is always negative.

In this way, the tangential winds were considered, where these winds are spirals cyclically around the system's eye, in the vicinity of the surface, but are spiraled anticyclonically near the top of the hurricane, that is, away from the system's eye. Then, the tangential velocity decreases with altitude and eventually changes the signal. Thus, the Ideal Gases Law was used, in order to show how the tangential component of the wind (V_{tan}) varies with the altitude (h), Eq.(7):

$$\left(\frac{2 \cdot V_{tan}}{R} + f_c\right) \cdot \frac{\Delta V_{tan}}{\Delta h} = \frac{g}{\bar{T}} \cdot \frac{\Delta T}{\Delta R} \quad (7)$$

where R is the radius, g the acceleration of gravity (9.8 m/s^2), and $\bar{T}$ the average temperature.

The reverse pressure derivation in relation to Eq. (6) was applied, obtaining the hypsometric equation to relate the pressure in the top of the hurricane's eye. Therefore, it was also applied to the surroundings of the eye, obtaining Eq.(8):

$$\Delta P_t = P_{b\infty} \cdot EXP\left[\frac{-g \cdot h_{max}}{(R \cdot \overline{T_\infty})}\right] - P_{be} \cdot EXP\left[\frac{-g \cdot h_{max}}{(R \cdot \overline{T_e})}\right] \quad (8)$$

in which, $P_b = (P_{b\infty} - \Delta P_b)$, where exponential terms are multiplied by $P_{b\infty}$. And finally, a first-order approach was used to these exponentials, generating Eq. (6). Where, $a = EXP[\frac{-g \cdot h_{max}}{(R \cdot \overline{T_e})}]$, where this value is approximated to 0.15, and $b = -[\frac{g \cdot h_{max} \cdot P_{b\infty}}{(R \cdot \overline{T_e} \cdot \overline{T_\infty})}]$, having approximate value of $0.7\ kPa/K$ ($7\ hPa/K$). Gravity acceleration (g), R the universal gas constant for dry air (R = 287.04 $m^2 s^{-2}\ K^{-1}$).

Although systems can be quite complex, the idealization of a model becomes necessary for a better understanding of the system. For example, one of the intensity measures of tropical cyclones is the pressure difference, according to Eq.(9):

$$\Delta P_{max} = P_\infty - P_e \quad (9)$$

Surface pressure distribution can be approximated by:

$$\frac{\Delta P}{\Delta P_{max}}\left\{\frac{1}{5} \cdot \left(\frac{R}{R_0}\right)^4 \rightarrow for\ R \leq R_0\ and\ \frac{\Delta P}{\Delta P_{max}}\right\}1 - \frac{4}{5} \cdot \frac{R_0}{R} \rightarrow for\ R > R_0 \quad (10)$$

In which $\Delta P = P(R) - P_e$, R is the radial distance from the center of the eye, R_0 is the critical radius where maximum tangential winds are identified. In this model, R_0 has twice the radius of the eye.

To form a hurricane, winds must be at least 33 $m.s^{-1}$ in the vicinity of the surface. It is important to mention that as the pressure at sea level in the hurricane's eye decreases, the maximum tangential winds (V_{max}) around the eye increase.

The maximum wind radius (V_{max}) refers to the distance from the center of the system to the location within its structure where vmax occurs. The maximum radius (R_{max}) plays a significant role in the characteristics of the system. Graham and Nunn (1959) suggested

to Eq. (11), where R_{max} is a function of latitude, a difference of central surface pressure and ambient pressure, as well as the speed of translation of the hurricane (Kalourazi et al., 2020).

$$R_{max} = 28.25 \cdot tang[0.0873 \cdot (\emptyset - 28) + 12.22 \cdot \exp\left(\frac{\Delta P_{max}}{33.86}\right) + 0.2 \cdot V_{max} + 37.2 \quad (11)$$

In which, $\emptyset$ is the latitude of the center of the hurricane, ΔP_{max} is the maximum pressure gradient (Eq. 9), and V_{max} the maximum wind obtained through $V_{max} = K(\Delta P_{max})^{\frac{1}{2}}$, being K = 13.4 is a proportionality constant (Atkinson and Holliday, 1977).

As the winds were considered cyclotrophic (drag against the sea surface and the Coriolis force were neglected), then the previous approach to pressure distribution (Eq. 11) was used to give a tangential velocity distribution near the surface.

$$\frac{V_{tan}}{V_{max}}\left\{(\frac{R}{R_0})^2 \rightarrow for\ R \leq R_0\ and\ \frac{V_{tan}}{V_{max}}\right\}\left\{\left(\frac{R_0}{R}\right)^{\frac{1}{2}} \rightarrow for\ R > R_0\right. \quad (12)$$

Where R_0 is the maximum speed occurs in the critical radius.

It is important to mention that the total wind speed relative to the surface is the vector sum of the translation speed and the speed of rotation.

4.2 RADIAL VELOCITY

In a hurricane, the air near the surface is "trapped" below the top of the PBL, with the air converging horizontally toward the eye wall (Merril, 1984), so horizontal continuity in cylindrical coordinates requires:

$$V_{rad} \cdot R = Constant \quad (13)$$

Where V_{rad} is the component of radial velocity, and negative for the influx. Therefore, it starts away from the hurricane, as *R* slows down toward R_0, and the magnitude of the influx should increase (Weatherford and Gray, 1988).

Eq. (14) considers the previous assumptions, and the relationship between the V_{rad} and the speed V_{max} according to the following equations:

$$\frac{V_{rad}}{V_{max}} = \left\{ -\frac{R}{R_0} \cdot \left[\frac{1}{5} \cdot \left(\frac{R}{R_0} \right)^3 + \frac{1}{2} \cdot \frac{\omega_S}{V_{max}} \cdot \frac{R_0}{h_i} \right] \right. \quad \rightarrow \quad for\ R \leq R_0 \tag{14a}$$

$$\frac{V_{rad}}{V_{max}} = \left\{ -\frac{R_0}{R} \cdot \left[\frac{1}{5} + \frac{1}{2} \cdot \frac{\omega_S}{V_{max}} \cdot \frac{R_0}{h_i} \right] \right. \quad \rightarrow \quad for\ R > R_0 \tag{14a}$$

Where, ω_S is negative and represents the average subsidence velocity in the hurricane's eye, i.e., the horizontal area of the eye, gives the total kinematic mass flow. The h_i is the depth of the boundary layer, being constant in 1000 m. While V_{max} is the maximum tangential speed.

4.3 VERTICAL SPEED

When the rays are smaller than R_0, the air converges quickly and accumulates, then ascends out of the PBL as convection inside the eye wall. Thus, the vertical velocity to the top of the PBL is represented by the equation of mass continuity, according to Eq. (15):

$$\frac{\omega}{V_{max}} = \left\{ \frac{h_i}{R_0} \cdot \left(\frac{R}{R_0} \right)^3 + \frac{\omega_s}{V_{max}} \right. \quad \rightarrow for\ R < R_0 \tag{15}$$

$\frac{\omega}{V_{max}} = 0$ for $R > R_0$.

For simplification, the upward movement in the regions where there is precipitation is neglected, that is, when $R > R_0$. In addition, ω_s is negative for subsidence. However, subsidence acts only within the eye, but the above ratio applies to all places within the R_0 to simplify.

4.4 THERMAL CONDITIONS

Assuming that the difference between the eye and the surroundings at the top of the hurricane is equal to and opposite to the bottom, generating Eq. (16):

$$\Delta T(R) = c \cdot [\Delta P_{max} - \Delta P(R)] \quad (16)$$

where, $c = 1.64 \frac{K}{kPa}$. The pressure difference at the bottom is $\Delta P = P(R) - P_e$, where the temperature difference calculated over the entire depth of the hurricane is (Rotunno and Emanuel, 1987): $\Delta T(R) = T_e - T(R)$, according to Eq. (17):

$$\frac{\Delta T}{\Delta T_{max}} = \left\{1 - \frac{1}{5}\left(\frac{R}{R_0}\right)^4 \quad \rightarrow \quad for\ R \leq R_0 \right. \quad (17a)$$

$$\frac{\Delta T}{\Delta T_{max}} = \left\{\frac{4}{5} \cdot \frac{R_0}{R} \quad \rightarrow \quad for\ R > R_0 \right. \quad (17b)$$

where, $\Delta T_{max} = T_e - T_\infty = c \cdot \Delta P_{max}$, e $c = 1.64 \frac{K}{kPa}$.

Entropy is another variable related to the activities of a hurricane because these systems are atmospheric structures that dissipate energy efficiently through irreversible processes. Bister and Emanuel (1998) mentioned that entropy in a hurricane grows by exchanging enthalpy of the sea surface in latent vaporization heat (lv) and by turbulent dissipation of kinetic energy in PBL.

The dynamic conditions required for the formation of a hurricane are related to low vertical wind shear, increased Coriolis force, and a convection trigger, through tropical atmospheric waves, tropospheric depressions (Tapiador et al., 2007). Therefore, the hurricane is a very efficient heat machine, which maintains itself, where it dissipates energy as efficiently as possible, but in order to occur, there has to be excess energy supply (Bister and Emanuel, 1998). In other words, hurricanes are efficient heat systems, or almost perfect machines in energy dissipation, removing enthalpy energy in the low troposphere and dissipating it through radiative restrained at the upper levels of the troposphere (Emanuel, 2003). Thus, the entropy condition (S) was introduced to the model to verify this thermal efficiency, according to Eq. (18):

$$S = c_p \cdot \ln\left(\frac{T}{T_0}\right) + \frac{l_v \cdot r}{T} - R \cdot \ln\left(\frac{P}{P_0}\right) \quad (18)$$

where, $c_p = 1004\, Jkg^{-1}K^{-1}$ is the specific heat of the air at a constant pressure, T is the absolute temperature, $l_v = 2500\, J/g_{water\ vapor}$ is the latent heat of vaporization, r is the mixing ratio, $R = 287\, Jkg^{-1}K^{-1}$ is the ideal gas constant, P is the pressure, $T_0 = 273.15$ K, and $P_0 = 1000$ hPa, are arbitrary reference values.

5. RESULTS AND DISCUSSION

5.1 PUNCTUAL ANALYSIS

Figure 1 shows the hurricane's Ike trajectory in September of 2008 based on the data available by the National Hurricane Center (*NHC*) - (NHC, 2008) and estimated by the model idealized in this work. It is important to mention that a geostrophic adjustment has been made in the field of Mean Sea Level Pressure (*MSLP*) to adjust the minimum pressure identified for a relationship close to the real, that is, the decay rate of this pressure is directly correlated with the relative cyclonic vorticity gain of the system, followed by the wind intensity, whether geostrophic or vertical. Furthermore, to make the criterion independent of latitude, the pressure decay rate was geostrophically adjusted for a given reference latitude, according to Eq. (19):

$$\frac{dP}{dt} = \left(\frac{dP}{dt}\right) \cdot \left(\frac{sen\varphi_{ref}}{sen\varphi}\right) \quad (19)$$

where $\frac{dP}{dt}$ represents the decay rate of the system, φ is the latitude of the center of the system, and φ_{ref} is the reference latitude, defined as 25°N.

When analyzing Figure 1, it was possible to identify similarity between the observed trajectory (red line) and that predicted by the idealized model (black line), except for dissimilarity between the trajectories close to the latitude of 23°N and longitude of 78°W, where the idealized model tends to anticipate and rewind the trajectory with the trajectory

of observation (red line). In the later trajectories, there was quite a similarity based on the Root-Mean-Square Error (*RMSE*) between positions and trajectories was of the order of 0.502°, which equates to approximately 98 miles or 157.7 km.

Regarding dynamic conditions such as azimuthal tangential velocity (Figure 2), again the idealized model could simulate the relationship between normalized tangential velocity and the radial distance also normalized for two distinct moments of the hurricane (0600 UTC on September 4th, 2008 – when the system is at its maximum intensity; and when the system reaches the coast, 1200 UTC on September 12th, 2008).

The first peak of the azimuthal tangential velocity occurred between 60 and 110 km from the center of the system, where the model (dashed orange line) anticipated this maximum to observation (blue line continues). After the maximum azimuthal tangential wind, there is a decrease in intensity when it moves away from the eye wall of the hurricane, but the model has an oscillation when compared to the observation (Wood and White, 2011).

Then, at 1200 UTC on September 12th, there was convergence in the maximum azimuthal tangential velocity of the model (dashed yellow line), and the observation (continuous lilac line) highlighted that the hurricane was already in the process of dissipating intensity (NHC, 2008).

Then, at 1200 UTC on September 12th, there was convergence in the maximum azimuthal tangential velocity of the model (dashed yellow line), and the observation (continuous lilac line) highlighted that the hurricane was already in the process of dissipating intensity (NHC, 2008). Therefore, the azimuthal tangential wind predicted by the idealized model appears as an important factor, which characterized similar oscillation as identified by the observation, that is, oscillation when moving away from the eye wall to the idealized model and linear decrease observed when it moves away from its maximum. The *RMSE* between the observation and the model idealized for 0600 UTC on September 4th, 2008

was 0.98 m/s and 0.99 m/s for 1200 UTC on September 12th, 2008. Thus, as we move away from the hurricane center, the vortex at the edge of the eye loses its effect, while speeds begin to follow a standard logarithmic profile, identified in Figure 2 at both times. In a hurricane, the air has mass and acquires tangential velocity when it enters the circulation at a certain distance from the system's center, where mass has angular momentum.

The angular moment of this air mass in the cyclonic circulation is preserved because only the external torque changes the angular momentum, and much of this torque is represented by the torques of friction with the sea surface itself (Vigh and Schubert, 2009; Knutson et al., 2019). As the air mass approaches the cyclonic center over time, the ascending air column acts as a "vacuum cleaner" resulting from the pressure gradient force and thus gains tangential velocity so that the angular momentum is conserved (Holland and Merrill, 1984; Knutson et al., 2019).

5.2 SPATIAL ANALYSIS

5.2.1 TANGENTIAL SPEED

The wind speed in a hurricane suffers asymmetry due to the system's advancing speed. A simple overlap of hurricane advancing speed and maximum wind drives the higher speeds of the hurricane's right side in the HN (Holland and Merrill, 1984). In Figure 3, between September 8th and 13th, the tangential winds were quite intense to the right of the hurricane's advance, to which this effect can be included in an asymmetric model. Another significant factor was the asymmetry in the drag force at the lower limit, due to the asymmetry of the wind speed due to the speed of advance of the hurricane, which introduces asymmetric convection and an asymmetric wind distribution in the PBL (Holland and Merrill, 1984).

425

426 5.2.2 MAXIMUM SPEED

427 In the idealized model, the height of the PBL delimited was 100 m. This procedure, along
428 with other dynamic forces, resulted in higher wind speed, as mentioned earlier on the
429 hurricane's right side in the HN. Shapiro (1983) identified this configuration by numerical
430 means, followed by Kepert (2001) by analytical method. Kepert (2001) used a solution
431 where PBL was disturbed in the conservation equation of momentum and, thus,
432 considered the drag forces and the vertical turbulent diffusion of the momentum. Another
433 factor identified in the study was d linked to the linear effect of the hurricane's advancing
434 velocity. The idealized model included using an exponential radial reduction coefficient,
435 as previously suggested by Schwerdt et al. (1979).

436 This condition previously mentioned was explained in Figure 4, where the maximum
437 velocity was identified to the right of the hurricane's trajectory. This maximum wind
438 (Vmax) is the vector sum of the translation speed and rotation speed. Therefore, in this
439 quadrant, the right of the translation allocation movement, it was identified that the Vmax
440 was present, and hurricanes are faster in this quadrant.

441 In the left part of the hurricane, the translation allocated velocity is subtracted from
442 tangential velocity so that the total or maximum velocity in this quadrant (left) is not as
443 intense as in the right quadrant. On September 12th, 0600 and 1200 UTC (Figure 4g, h)
444 identified this condition, with greater intensity in the right quadrant of Hurricane Ike
445 (Figure 4).

446

447 5.2.3 RADIAL SPEED

448 When idealizing a hurricane, it is known that PBL air is confined below the top of this
449 layer, as the air converges horizontally towards the eye wall (Ghosh and Chakravarty,

2018). As the wind speed increases in the direction of the eye wall, the height of the sea surface tends to "couple" radial and tangential velocities. Figure 5 shows a higher radial velocity located in the right quadrant of the system's direction of displacement. This configuration can occur due to a drag-induced influx between air and the sea surface. This influx eventually converges the ascent through the PBL and radial pumping process. As a result, vertical velocity and relative vorticity move radially out, reinforcing that this configuration was identified in Figure 5, following the asymmetric conservation of surface drag, according to Shapiro (1983).

5.2.4 EKMAN TRANSPORT

Ekman's spiral describes how the current direction and velocity vary with depth. The Ekman's liquid transport accumulated at all depths is perpendicular to the surface wind direction. As with the radial velocity in NH, the liquid transport of seawater is to the right of the maximum wind (Vincent et al., 2013). Then, as the hurricane approaches the continent, winds along its front and right edge become almost parallel to the coast (Figure 6), and consequently, there is a liquid Ekman's transport directly to the coast.

If the hurricane "hovered" along the coast long enough to allow the development of a steady-state condition, thus, Ekman's transport toward the coast would be balanced by the slope of the swell (Vincent et al., 2013). This process shown by the idealized model (Figure 6) corroborates with the results obtained by Jullien et al. (2012). In addition, the authors suggest that the winds of a hurricane intensify the wind strain wave in the center of a hurricane's basin and thus contribute to a background Ekman pumping (Bueti et al., 2014).

Furthermore, it is worth noting that the influence of Ekman's transport was not deepened in the study. However, it was necessary, especially in oceanic conditions, due to the

displacement of the thermocline after the passage of a storm resembles Ekman's solution, as suggested by Gill (1982) in an inertial oscillation.

As a hurricane has a high range, the most relevant Ekman transport is in the quadrant to the right of the hurricane shift. In this way, the amount of water accumulates higher between the hurricane and the continental coast and south of the system (Figure 6), this creates waves, and these waves always travel with the coast to their right (Figure 6g, h), so that there is a higher amplitude.

5.2.5 ENTROPY

The maximum increase in moist entropy and the tropopause temperature determines the wind speed on the eye wall. The energy production of *LE* and sensitive (*H*) flows because more heat generated by viscous dissipation applies and balances friction dissipation (Bister and Emanuel, 1998).

High SST values increase the balance of moist air entropy (S*) and energy production under the eye wall (Emanuel, 1995). However, the imbalance of wet entropy on the eye wall was also influenced by the air thermodynamic characteristics when it approaches the eye wall. Therefore, the flow of air entering the eye wall region with higher wet entropy will have a minor imbalance in the ocean-atmosphere system and less energy production under the eye wall.

Figure 7 displays entropy for the period September 8-13th, 2008. There is a "pocket" of entropy around the hurricane's eye (with variations between 400 to 402 $J.kg^{-1}.K^{-1}$). This process showed the thermal efficiency of the hurricane because it converts thermal energy into mechanical energy (Emanuel, 1995).

Thus, by assuming the eye wall is in the Maximum Wind Radius (MWR). Outside the MWR, the air temperature is radially constant, as the flow of H to air over the ocean,

which in turn balances gradual adiabatic cooling as a function of decreased pressure. Therefore, it is worth noting that Relative Humidity (*RH*) remained with its environmental values outside the MWR once that it was identified that the air moisture flows over the ocean were balanced by the turbulent flows at the top of PBL.

6. CONCLUSIONS

Hurricane Ike's passage resulted in 80 fatalities and a loss of more than US$ 4 billion (NHC, 2008) across the Caribbean and the southeastern United States. Therefore, like every hurricane, predictability is paramount for preventing loss of life and property damage. To this end, the idealized model based on parametric formulations fed from initial conditions (ERA5 reanalysis) showed similarity in the trajectory between the geographic coordinates of the minimum pressure during the life of the hurricane with the lowest error (RMSE = 0.502° - 157 km).

The relationship between observation and prediction by the azimuthal tangential velocity model is satisfactory mainly in the eye wall, with lower errors obtained. However, it is noteworthy that the idealized model identified a decrease in wind intensity after reaching the maximum azimuthal tangential wind.

Spatially, the highest tangential velocities occur on the hurricane's right side, directly related to the drag force's asymmetry due to the hurricane's advance, which the idealized model well represented.

The maximum winds occurred to the right of the hurricane's trajectory due the cyclonic movement of the hurricane and a radial exponent reduction, as shown by the idealized model. In addition, this simple model presented satisfactory results for a Category 4 Hurricane, which can be very useful in weather forecasting centers around the world in identifying and assessing hurricanes.

7. REFERENCES

Atkinson, G. D., and Holliday, C. R. (1977). Tropical cyclone minimum sea level pressure/maximum sustained wind relationship for the western North Pacific. *Monthly Weather Review*, *105*(4), 421-427. https://doi.org/10.1175/1520-0493(1977)105<0421:TCMSLP>2.0.CO;2

Bauer, P., Thorpe, A., and Brunet, G. (2015). The quiet revolution of numerical weather prediction.*Nature*, *525*(7567), 47-55. https://doi.org/10.1038/nature14956

Bhardwaj, P., Singh, O. and Yadav, R.B.S. (2020). Probabilistic assessment of tropical cyclones' extreme wind speed in the Bay of Bengal: implications for future cyclonic hazard.*Natural Hazards* 01, 275–295. https://doi.org/10.1007/s11069-020-03873-5

Bister, M., and Emanuel, K. A. (1998). Dissipative heating and hurricane intensity.*Meteorology and Atmospheric Physics*,*65*(3), 233-240. https://doi.org/10.1007/BF01030791

Bryan, G. H., and Rotunno, R. (2009). Evaluation of an analytical model for the maximum intensity of tropical cyclones. *Journal of the Atmospheric Sciences*, *66*(10), 3042-3060. https://doi.org/10.1175/2009JAS3038.1

Bueti, M. R., Ginis, I., Rothstein, L. M., and Griffies, S. M. (2014). Tropical cyclone–induced thermocline warming and its regional and global impacts. *Journal of Climate*,*27*(18), 6978-6999. https://doi.org/10.1175/JCLI-D-14-00152.1

Chavas, D. R., and Lin, N. (2016). A model for the complete radial structure of the tropical cyclone wind field. Part II: Wind field variability. *Journal of Atmospheric Sciences*,*73*(8), 3093-3113. https://doi.org/10.1175/JAS-D-15-0185.1

Davis, C. A. (2018). Resolving tropical cyclone intensity in models. *Geophysical Research Letters*, *45*, 2082– 2087. https://doi.org/10.1002/2017GL076966

549 Emanuel, K. A. (1995). The behavior of a simple hurricane model using a convective
550 scheme based on subcloud-layer entropy equilibrium. *Journal of Atmospheric*
551 *Sciences*,*52*(22), 3960-3968. https://doi.org/10.1175/1520-
552 0469(1995)052<3960:TBOASH>2.0.CO;2
553 Emanuel, K. (2003). Tropical cyclones. *Annual review of earth and planetary sciences*,
554 *31*(1), 75-104. https://doi.org/10.1146/annurev.earth.31.100901.141259
555 Emanuel K. A. (2004). Tropical cyclone energetics and structure. In: Atmospheric
556 Turbulence and Mesoscale Meteorology, Fedorovich E, Rotunno R, Stevens B. (eds.)
557 Cambridge University Press, p.165–191.
558 Emanuel, K., and Rotunno, R. (2011). Self-stratification of tropical cyclone outflow. Part
559 I: Implications for storm structure. *Journal of the Atmospheric Sciences*, *68*(10), 2236-
560 2249. https://doi.org/10.1175/JAS-D-10-05024.1
561 Elsner, J. B., Elsner, G. J. B., and Kara, A. B. (1999). *Hurricanes of the North Atlantic:*
562 *Climate and society*. Oxford University Press on Demand.
563 Ghosh, I., and Chakravarty, N. (2018). Tropical cyclone: expressions for velocity
564 components and stability parameter. *Natural Hazards*, *94*(3), 1293-1304.
565 https://doi.org/10.1007/s11069-018-3477-7
566 Gleckler, P. J., Taylor, K. E., and Doutriaux, C. (2008). Performance metrics for climate
567 models. *Journal of Geophysical Research: Atmospheres*, *113*(D6).
568 https://doi.org/10.1029/2007JD008972
569 Graham, H. E., and Nunn, D. E. (1959). Meteorological conditions pertinent to standard
570 project hurricane. *Atlantic and Gulf Coasts of United States. Weather Bureau, US*
571 *Department of Commerce, Washington, DC*.
572 Harasti, P. R. (2003). The hurricane volume velocity processing method. In *Preprints,*
573 *31st Conf. on Radar Meteorology, Seattle, WA, Amer. Meteor. Soc* (Vol. 1008, p. 1011).

574 Hart, R. E. (2003). A cyclone phase space derived from thermal wind and thermal
575 asymmetry. *Monthly Weather Review*, *131*(4), 585-616. https://doi.org/10.1175/1520-
576 0493(2003)131<0585:ACPSDF>2.0.CO;2
577 Hersbach, H. et al. (2020). The ERA5 global reanalysis. *Quarterly Journal of the Royal*
578 *Meteorological Society*, *146*(730), 1999-2049. https://doi.org/10.1002/qj.3803
579 Holland, G.J. An analytic model of the wind and pressure profiles in hurricanes. *Monthly*
580 *Weather Review*, *108*(1980), 1212-1218. https://doi.org/10.1175/1520-
581 0493(1980)108<1212:AAMOTW>2.0.CO;2
582 Holland, G. J., and Merrill, R. T. (1984). On the dynamics of tropical cyclone structural
583 changes. *Quarterly Journal of the Royal Meteorological Society*, *110*(465), 723-745.
584 https://doi.org/10.1002/qj.49711046510
585 Holland, G. J., Belanger, J. I., and Fritz, A. (2010). A revised model for radial profiles of
586 hurricane winds. *Monthly Weather Review*, *138*(12), 4393-4401.
587 https://doi.org/10.1175/2010MWR3317.1
588 Hu, K., Chen, Q., and Kimball, S. K. (2012). Consistency in hurricane surface wind
589 forecasting: an improved parametric model. *Natural Hazards*, *61*(3), 1029-1050.
590 https://doi.org/10.1007/s11069-011-9960-z
591 Jullien, S., Menkès, C. E., Marchesiello, P., Jourdain, N. C., Lengaigne, M., Koch-
592 Larrouy, A, Faure, V. (2012). Impact of tropical cyclones on the heat budget of the South
593 Pacific Ocean. *Journal of Physical Oceanography*, *42*(11), 1882-1906.
594 https://doi.org/10.1175/JPO-D-11-0133.1
595 Kalourazi, M. Y., Siadatmousavi, S. M., Yeganeh-Bakhtiary, A., and Jose, F. (2020).
596 Simulating tropical storms in the Gulf of Mexico using analytical models. *Oceanologia*,
597 *62*(2), 173-189. https://doi.org/10.1016/j.oceano.2019.11.001

598 Kalnay, E., Atmospheric Modeling, Data Assimilation, and Predictability (Cambridge
599 University Press, 2003).
600 Kepert, J. (2001). The dynamics of boundary layer jets within the tropical cyclone core.
601 Part I: Linear theory. *Journal of the Atmospheric Sciences*, *58*(17), 2469-2484.
602 https://doi.org/10.1175/1520-0469(2001)058<2469:TDOBLJ>2.0.CO;2
603 Knaff, J. A., Sampson, C. R., DeMaria, M., Marchok, T. P., Gross, J. M., and McAdie,
604 C. J. (2007). Statistical tropical cyclone wind radii prediction using climatology and
605 persistence. *Weather and Forecasting*, *22*(4), 781-791.
606 https://doi.org/10.1175/WAF1026.1
607 Knutson, T., Camargo, S. J., Chan, J. C. L., Emanuel, K., Ho, C., Kossin, J., Mohapatra,
608 M., Satoh, M., Sugi, M., Walsh, K., and Wu, L. (2019). Tropical Cyclones and Climate
609 Change Assessment: Part I: Detection and Attribution, *Bulletin of the American*
610 *Meteorological Society*, *100*(10), 1987-2007. https://doi.org/10.1175/BAMS-D-18-
611 0189.1
612 Knutson, T., Camargo, S. J., Chan, J. C. L., Emanuel, K., Ho, C., Kossin, J., Mohapatra,
613 M., Satoh, M., Sugi, M., Walsh, K., and Wu, L. (2020). Tropical Cyclones and Climate
614 Change Assessment: Part II: Projected Response to Anthropogenic Warming, *Bulletin of*
615 *the American Meteorological Society*, *101*(3), E303-E322.
616 https://doi.org/10.1175/BAMS-D-18-0189.1
617 Lin, N., and Chavas, D. (2012). On hurricane parametric wind and applications in storm
618 surge modeling. *Journal of Geophysical Research: Atmospheres*, *117*(D9).
619 https://doi.org/10.1029/2011JD017126
620 Luitel, B., Villarini, G., and Vecchi, G. A. (2018). Verification of the skill of numerical
621 weather prediction models in forecasting rainfall from US landfalling tropical cyclones.
622 *Journal of Hydrology*, *556*, 1026-1037. https://doi.org/10.1016/j.jhydrol.2016.09.019

623 Malkus, J. S., and Riehl, H. (1960). On the dynamics and energy transformations in
624 steady-state hurricanes. *Tellus*, *12*(1), 1-20. https://doi.org/10.3402/tellusa.v12i1.9351
625 Martinez, A. B. (2020). Improving normalized hurricane damages. *Nature Sustainability*,
626 *3*(7), 517-518. https://doi.org/10.1038/s41893-020-0550-5.
627 Mattocks, C., and Forbes, C. (2008). A real-time, event-triggered storm surge forecasting
628 system for the state of North Carolina. *Ocean Modelling*, *25*(3-4), 95-119.
629 https://doi.org/10.1016/j.ocemod.2008.06.008
630 Merrill, R. T. (1984). A comparison of large and small tropical cyclones. *Monthly*
631 *Weather Review*, *112*(7), 1408-1418. https://doi.org/10.1175/1520-
632 0493(1980)108,1212:AAMOTW.2.0.CO;2
633 Olfateh M., Callaghan D.P., Nielsen P., Baldock T.E. **Tropical cyclone wind field**
634 **asymmetry-development and evaluation of a new parametric model.** *Journal*
635 *Geophysical Research Oceans*, *122*(2017), 458-469.
636 https://doi.org/10.1002/2016JC012237
637 Osuri, K. K., Mohanty, U. C., Routray, A., Mohapatra, M., and Niyogi, D. (2013). Real-
638 time track prediction of tropical cyclones over the North Indian Ocean using the ARW
639 model.*Journal of Applied Meteorology and Climatology*,*52*(11), 2476-2492.
640 Powell, M. D., and Reinhold, T. A. (2007). Tropical cyclone destructive potential by
641 integrated kinetic energy.*Bulletin of the American Meteorological Society*, *88*(4), 513-
642 526.
643 Rotunno, R., and Emanuel, K. A. (1987). An air–sea interaction theory for tropical
644 cyclones. Part II: Evolutionary study using a nonhydrostatic axisymmetric numerical
645 model. *Journal of Atmospheric Sciences*,*44*(3), 542-561. https://doi.org/10.1175/1520-
646 0469(1987)044<0542:AAITFT>2.0.CO;2

Schloemer, R. W. (1954). Analysis and synthesis of hurricane wind patterns over Lake Okechobee.*Florida US Weather Bureau, Hydromet. Rep.*, *31*, 1-49.

Schwerdt, R. W., Ho, F. P., and Watkins, R. R. (1979). Meteorological criteria for standard project hurricane and probable maximum hurricane windfields, Gulf and East Coasts of the United States. NOAA Tech. Rep. NWS 23, 317 pp. [Available from National Hurricane/Tropical Prediction Center Library, 11691 S.W. 117th St., Miami, FL 33165-2149.].

Shapiro, L. J. (1983). The asymmetric boundary layer flow under a translating hurricane. *Journal of Atmospheric Sciences*, *40*(8), 1984-1998. https://doi.org/10.1175/1520-0469(1983)040<1984:TABLFU>2.0.CO;2

Smith, R. K. (1980). Tropical cyclone eye dynamics. *Journal of Atmospheric Sciences*, *37*(6), 1227-1232. https://doi.org/10.1175/1520-0469(1980)037<1227:TCED>2.0.CO;2.

Takagi, H., Nguyen, D. T., Esteban, M. I. G. U. E. L., Tran, T. T., Knaepen, H. L., and Mikami, T. A. K. (2012, October). Vulnerability of coastal areas in Southern Vietnam against tropical cyclones and storm surges. In: *The 4th International Conference on Estuaries and Coasts (ICEC2012)*-(pp. 8-pp).

Tang, B., and Emanuel, K. (2012). A ventilation index for tropical cyclones. *Bulletin of the American Meteorological Society*, *93*(12), 1901-1912. https://doi.org/10.1175/BAMS-D-11-00165.1.

Tapiador, F. J., Gaertner, M. A., Romera, R., and Castro, M. (2007). A multisource analysis of Hurricane Vince. *Bulletin of the American Meteorological Society*, *88*(7), 1027-1032. https://doi.org/10.1175/BAMS-88-7-1027

Váňa, F., Düben, P., Lang, S., Palmer, T., Leutbecher, M., Salmond, D., and Carver, G. (2017). Single precision in weather forecasting models: An evaluation with the IFS. *Monthly Weather Review*, *145*(2), 495-502. https://doi.org/10.1175/MWR-D-16-0228.1

672 Vickery, P. J., and Twisdale, L. A. (1995). Wind-field and filling models for hurricane
673 wind-speed predictions. *Journal of Structural Engineering*, *121*(11), 1700-1709.
674 https://doi.org/10.1061/(ASCE)0733-9445(1995)121:11(1700)
675 Vickery, P. J. (2005). Simple empirical models for estimating the increase in the central
676 pressure of tropical cyclones after landfall along the coastline of the United States.
677 *Journal of Applied Meteorology*, *44*(12), 1807-1826. https://doi.org/10.1175/JAM2310.1
678 Vickery, P. J., and Wadhera, D. (2008). Statistical models of Holland pressure profile
679 parameter and radius to maximum winds of hurricanes from flight-level pressure and H*
680 Wind data. *Journal of Applied Meteorology and Climatology*,*47*(10), 2497-2517.
681 https://doi.org/10.1175/2008JAMC1837.1
682 Vickery, P. J., Masters, F. J., Powell, M. D., and Wadhera, D. (2009). Hurricane hazard
683 modeling: The past, present, and future.*Journal of Wind Engineering and Industrial*
684 *Aerodynamics*, *97*(7-8), 392-405. https://doi.org/10.1016/j.jweia.2009.05.005
685 Vigh, J. L., and Schubert, W. H. (2009). Rapid development of the tropical cyclone warm
686 core. *Journal of the Atmospheric Sciences*, *66*(11), 3335-3350.
687 https://doi.org/10.1175/2009JAS3092.1
688 Vigh, J. L., Knaff, J. A., and Schubert, W. H. (2012). A climatology of hurricane eye
689 formation. *Monthly Weather Review*, *140*(5), 1405-1426. https://doi.org/10.1175/MWR-
690 D-11-00108.1.
691 Vincent, E. M., Madec, G., Lengaigne, M., Vialard, J., and Koch-Larrouy, A. (2013).
692 Influence of tropical cyclones on sea surface temperature seasonal cycle and ocean heat
693 transport. *Climate Dynamics*, *41*(7-8), 2019-2038. https://doi.org/10.1007/s00382-012-
694 1556-0

Wang, C., Zhang, H., Feng, K., and Li, Q. (2017). A simple gradient wind field model for translating tropical cyclones. *Natural Hazards*, *88*(1), 651-658. https://doi.org/10.1007/s11069-017-2882-7

Warner, T. T. (2010). *Numerical weather and climate prediction*. cambridge university press.

Weatherford, C. L., and Gray, W. M. (1988). Typhoon structure as revealed by aircraft reconnaissance. Part II: Structural variability. *Monthly Weather Review*, *116*(5), 1044-1056. https://doi.org/10.1175/1520-0493(1988)116<1044:TSARBA>2.0.CO;2

Willoughby, H. E., and Rahn, M. E. (2004). Parametric representation of the primary hurricane vortex. Part I: Observations and evaluation of the Holland (1980) model. *Monthly Weather Review*, *132*(12), 3033-3048. https://doi.org/10.1175/MWR2831.1

Wood, V. T., and White, L. W. (2011). A new parametric model of vortex tangential-wind profiles: Development, testing, and verification. *Journal of the Atmospheric Sciences*, *68*(5), 990-1006. https://doi.org/10.1175/2011JAS3588.1

Xie, L., Bao, S., Pietrafesa, L. J., Foley, K., and Fuentes, M. (2006). A real-time hurricane surface wind forecasting model: Formulation and verification. *Monthly Weather Review*, *134*(5), 1355-1370. https://doi.org/10.1175/MWR3126.1

Xie, L., Liu, H., Liu, B., and Bao, S. (2011). A numerical study of the effect of hurricane wind asymmetry on storm surge and inundation. *Ocean Modelling*, *36*(1-2), 71-79. https://doi.org/10.1016/j.ocemod.2010.10.001

Yoshizumi, S. (1968). On the asymmetry of wind distribution in the lower layer in typhoon. *Journal of the Meteorological Society of Japan. Ser. II*, *46*(3), 153-159. https://doi.org/10.2151/jmsj1965.46.3_153

718 Zhao, M., and Held, I. M. (2010). An analysis of the effect of global warming on the
719 intensity of Atlantic hurricanes using a GCM with statistical refinement.*Journal of*
720 *Climate*,*23*(23), 6382-6393. https://doi.org/10.1175/2010JCLI3837.1
721 Yoshizumi, S. (1968). On the asymmetry of wind distribution in the lower layer in
722 typhoon. *Journal of the Meteorological Society of Japan. Ser. II*, *46*(3), 153-159.
723 https://doi.org/10.2151/jmsj1965.46.3_153
724 Zhao, M., and Held, I. M. (2010). An analysis of the effect of global warming on the
725 intensity of Atlantic hurricanes using a GCM with statistical refinement. *Journal of*
726 *Climate*, *23*(23), 6382-6393. https://doi.org/10.1175/2010JCLI3837.1
727
728
729
730
731
732
733
734
735
736
737
738
739
740
741
742

743 **FIGURE CAPTIONS**

744 **Figure 1** – Observed trajectory (red line) and predicted by the idealized model (black
745 line) of Hurricane Ike, between 3 and 12 September 2008.

746 **Figure 2** – Normalized radial wind velocity (m.s-1) and normalized radial distance (km)
747 for two different days. 0600 UTC – September 4th (observed – Blue line; Model – Orange
748 dashed line) and 1200 UTC – September 12th (observed – Lilac line; Model – Yellow
749 dashed line).

750 **Figure 3** – Tangential Wind (m/s) around hurricane Ike, 0000 UTC 08 September 2008
751 to 0000 UTC 13 September 2008. The *m* and *n* are zoom for around hurricane in 0600
752 and 1200 UTC 12 September 2008.

753 **Figure 4** – Maximum Wind (m/s) around hurricane Ike, 0000 UTC 08 September 2008
754 to 0000 UTC 13 September 2008. The *m* and *n* are zoom for around hurricane in 0600
755 and 1200 UTC 12 September 2008.

756 **Figure 5** – Radial wind ($m.s^{-1}$) around hurricane Ike, 0000 UTC 08 September 2008 to
757 0000 UTC 13 September 2008. The *m* and *n* are zoom for around hurricane in 0600 and
758 1200 UTC 12 September 2008.

759 **Figure 6** – Ekman Transport (m^2/s) around hurricane Ike, 0000 UTC 08 September 2008
760 to 0000 UTC 13 September 2008. The *m* and *n* are zoom for around hurricane in 0600
761 and 1200 UTC 12 September 2008.

762 **Figure 7** – Entropy ($J\ kg^{-1}\ K^{-1}$) around hurricane Ike, 0000 UTC 08 September 2008 to
763 0000 UTC 13 September 2008. The *m* and *n* are zoom for around hurricane in 0600 and
764 1200 UTC 12 September 2008.

765 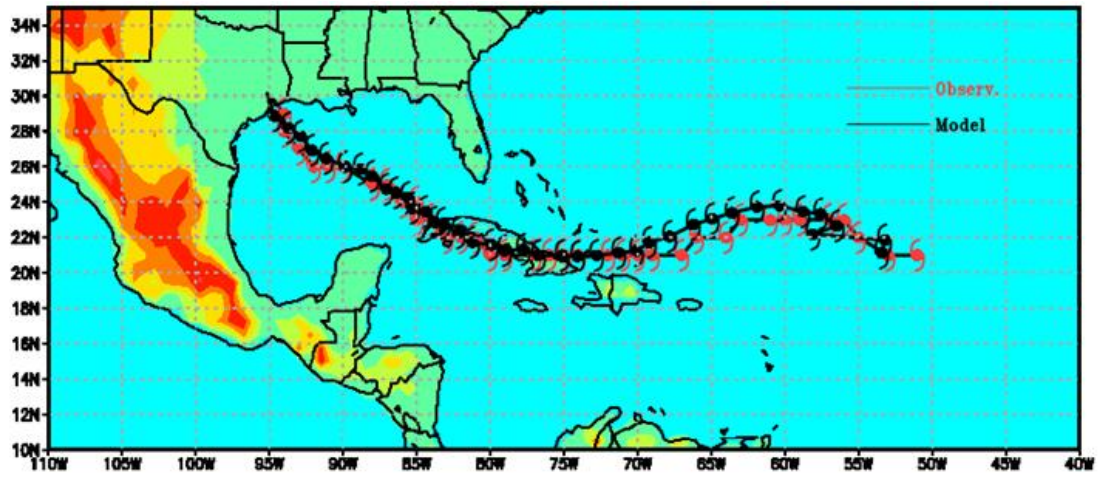

766 Figure 1

767

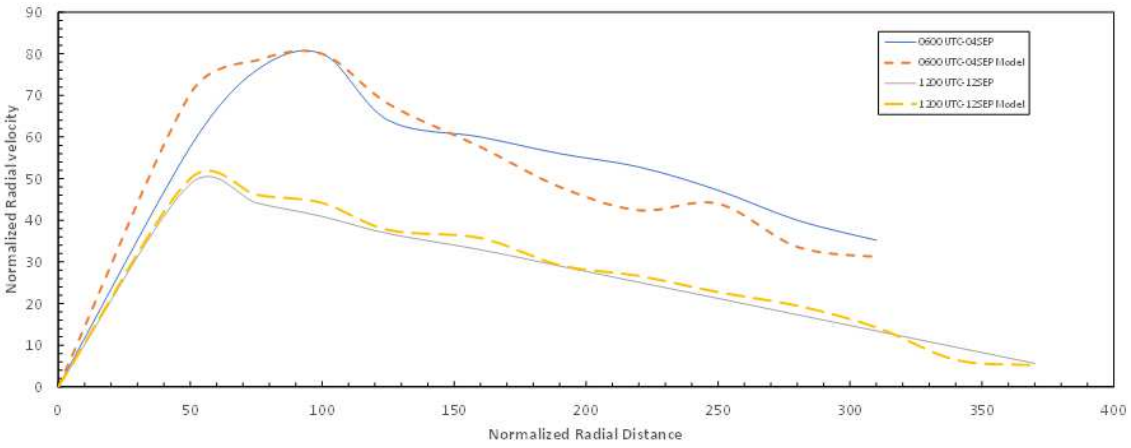

768

769 Figure 2

770

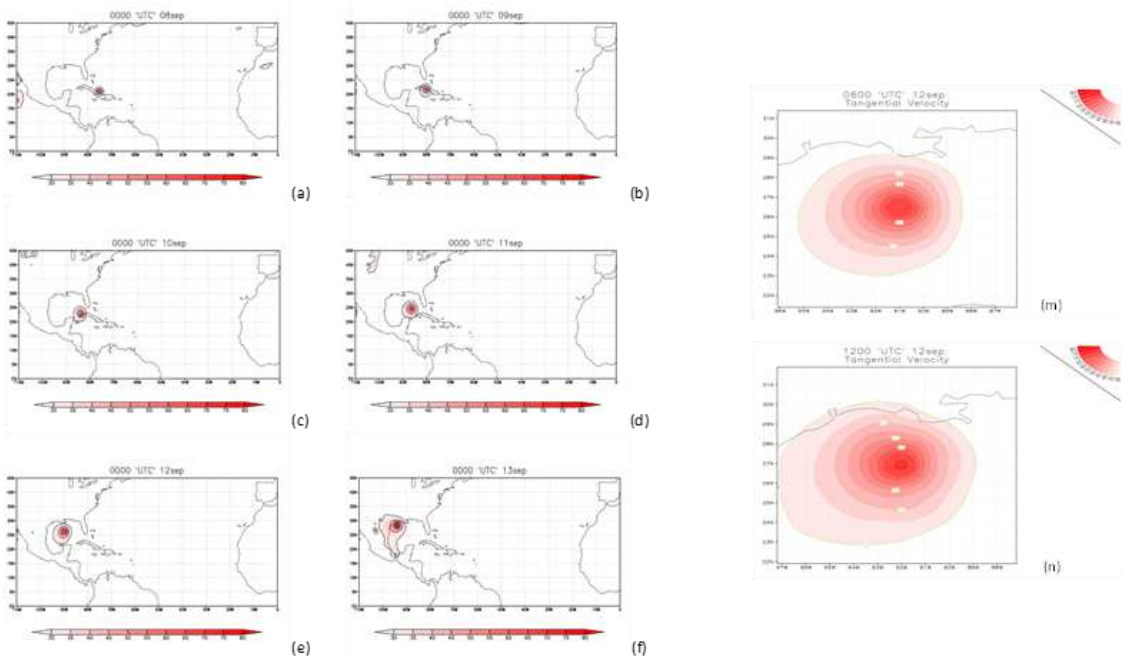

771

772 Figure 3

773

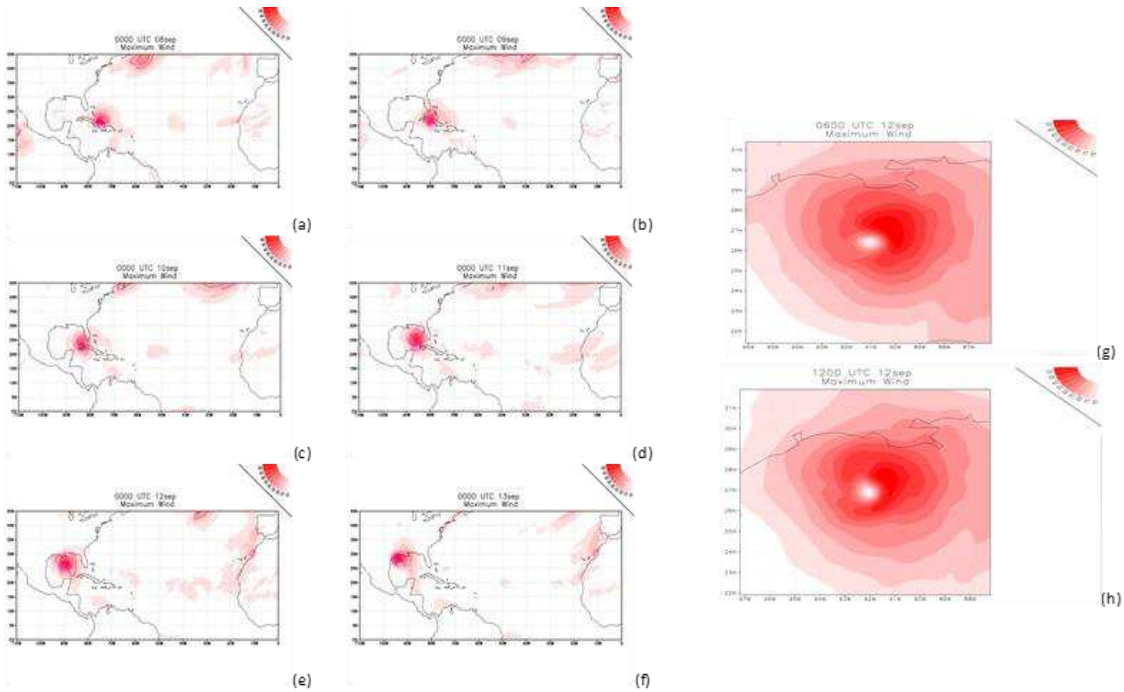

774

775 Figure 4

776

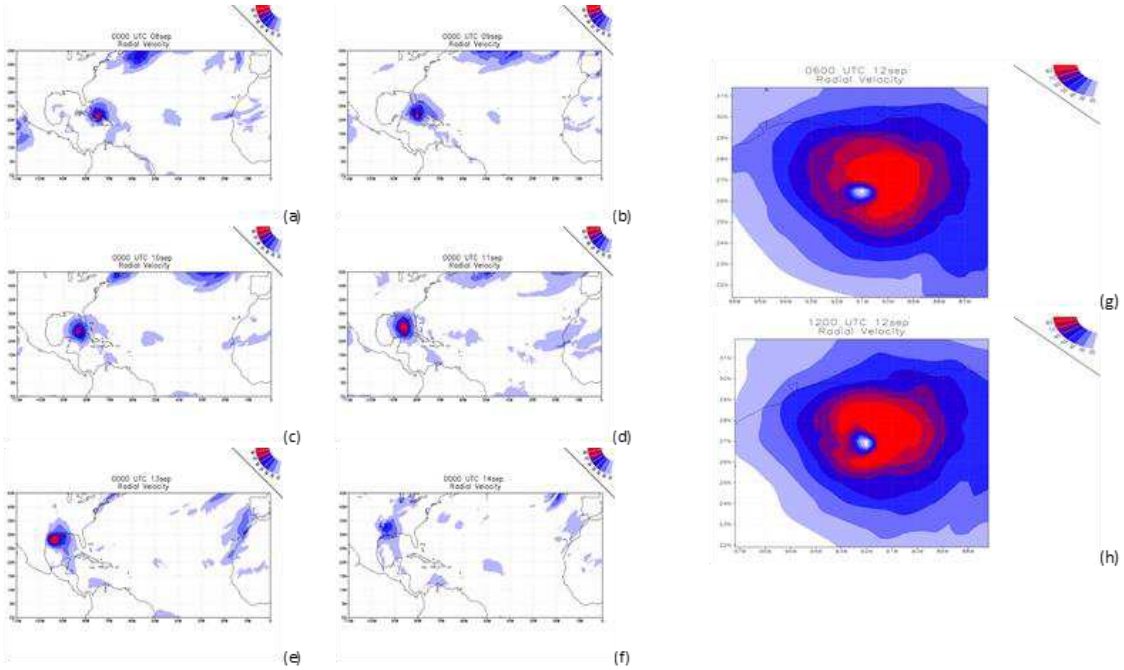

777

778 Figure 5

779

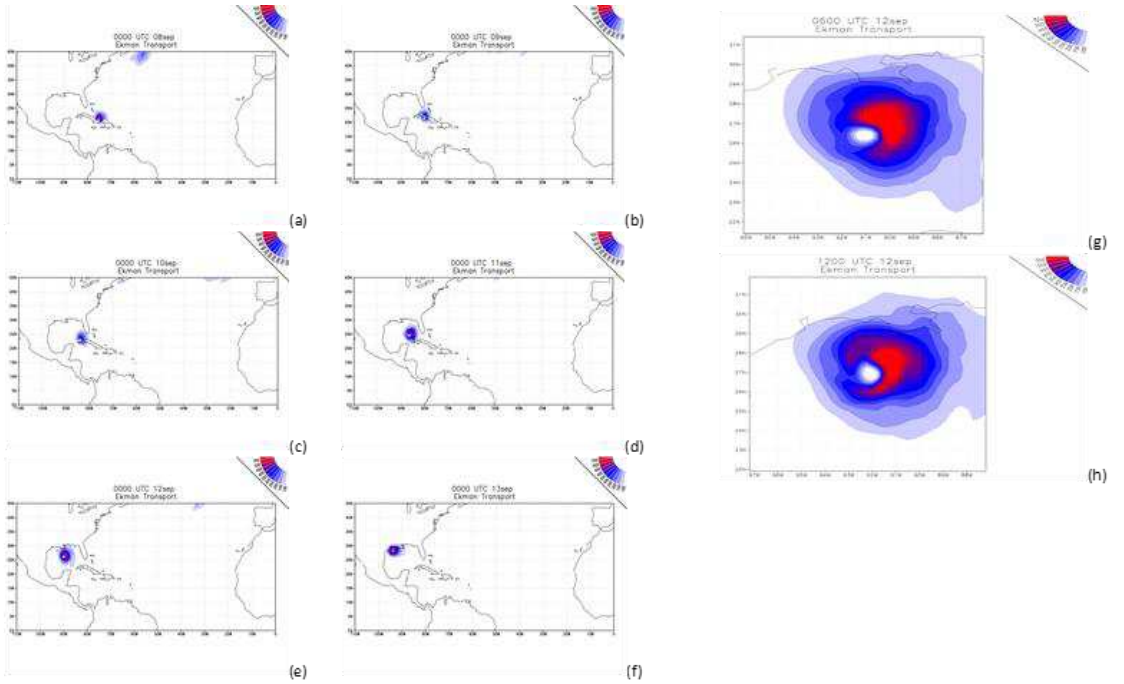

780

781 Figure 6

782

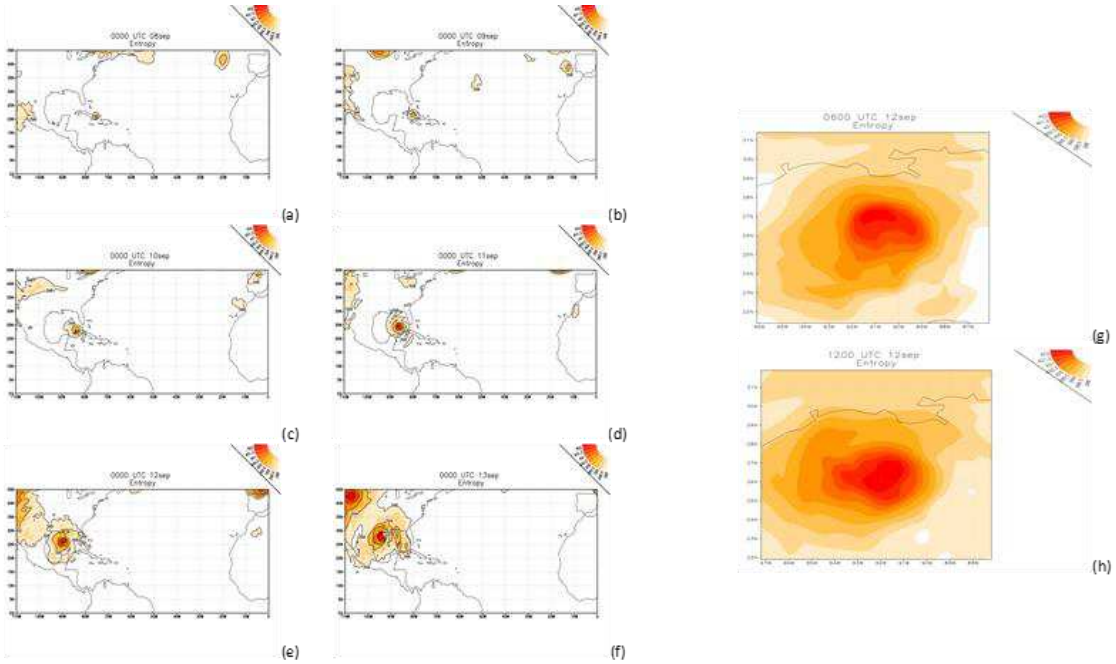

783

784 Figure 7

785